Physical Education, Health and Social Sciences
https://journal-of-social-education.org
E-ISSN: 2958-5996
P-ISSN: 2958-5988


# Halide-Engineered Multifunctionality in Lead-Free $Cs_2AlTlX_6$ (X = I, F) Double Perovskites: A First-Principles Study of Structural, Optoelectronic, Elastic, and Thermoelectric Properties

Fareesa Tasneem Tahir[1*], Laiba Saqib Khalil[2], Mohammed Hussein Abdullah[2], Shahzad Khan[2], Tahir Khalil[2], Rani Khattak[2], Laiq Zada[2], Faizan Ahmad Khan[3], Haroon[2], Aziz Ullah[4]

[1] College of Physics and optical engineering, State Key Laboratory of Radio Frequency Heterogeneous Integration, Shenzhen University, Shenzhen 518060, Guangdong, P.R. China.
[2] Department of Physics, University of Peshawar, Peshawar 25120, Khyber Pakhtunkhwa, Pakistan.
[3] Department of Physics, Islamia College, Peshawar 25120, Khyber Pakhtunkhwa, Pakistan.
[4] Department of Physics, Qurtaba University of Science and Information Technology, Peshawar 25100, Pakistan.
Corresponding author: Dr. Fareesa Tasneem Tahir (fareesatahir@gmail.com)
***DOI: https://doi.org/10.63163/jpehss.v4i1.1271***

## Abstract
Lead-free double perovskites have emerged as promising materials for next-generation optoelectronic and energy-conversion technologies because of their chemical tunability, structural stability, and multifunctional physical properties. In this study, the structural, elastic, electronic, optical, and thermoelectric properties of cubic $Cs_2AlTlX_6$ (X = I, F) double perovskites were scientifically explored using density functional theory. Structural optimization within the PBE-GGA framework confirms that both compounds are stable in the cubic Fm-3m phase, with $Cs_2AlTlI_6$ exhibiting a larger lattice constant and unit-cell volume, whereas $Cs_2AlTlF_6$ shows a higher bulk modulus and stronger mechanical rigidity. Elastic-constant analysis satisfies the Born–Huang stability criteria for both systems, indicating mechanical stability; $Cs_2AlTlI_6$ displays brittle behavior, while $Cs_2AlTlF_6$ exhibits comparatively greater stiffness and marginal ductile character. Electronic properties were analyzed using the TB-mBJ potential reveal indirect band gaps of 2.97 eV for $Cs_2AlTlI_6$ and 7.8 eV for $Cs_2AlTlF_6$, classifying the iodide compound as a semiconductor and the fluoride analogue as a wide-band-gap insulator. Optical analysis over the 0–40 eV photon-energy range demonstrates pronounced dielectric response, optical conductivity, absorption, refractive-index variation, reflectivity, extinction, and energy-loss features, indicating potential for visible–UV and ultraviolet photonic applications. Thermoelectric transport calculations further show that $Cs_2AlTlI_6$ possesses a large positive Seebeck coefficient, an enhanced power factor, and an almost temperature-independent figure of merit close to unity over 100–1000 K, whereas $Cs_2AlTlF_6$ exhibits weak thermoelectric efficiency despite its higher electrical conductivity because of its negligible thermopower. Overall, halide substitution strongly governs the multifunctional response of $Cs_2AlTlX_6$, with $Cs_2AlTlI_6$ emerging as the more favorable candidate for thermoelectric and optoelectronic applications, while $Cs_2AlTlF_6$ appears more suitable for ultraviolet optical environments requiring greater mechanical robustness.

**Keywords:** Lead-free double perovskites, Density functional theory, WIEN2k, ultraviolet photonics.

## Introduction
Hybrid organic-inorganic perovskite solar cells have demonstrated tremendous success and scientific interest in recent years and are an important development in the modern energy technologies [1, 2]. The perovskites of metal-halides have emerged as a relatively unknown material class only to become one of the most intensively studied material classes in an alarmingly brief amount of time. The efficiency of power conversion of perovskite-based solar cell has risen significantly, with the first design being dye-sensitized solar cells which had an efficiency of 3.8% [2] and the most recent

design of planar heterojunction devices reported by NREL at 20.1% efficiency [3]. Perovskite materials are known to have outstanding optoelectronic characteristics, such as tunable band gaps, high absorption coefficients, broad absorption spectra, high quantum yield of photoluminescence (PLQY), large charge carrier mobilities, long charge carrier diffusion lengths, and defect tolerance [4]. Perovskite materials, also, can be effectively tuned in adjusting their band gap by changing their composition, particularly, by the judicious addition and concentration of dopant materials. [5]. Examples of optoelectronic devices that have metal halide perovskite (MHP) include solar cells, photodetectors, and light-emitting diodes (LEDs). The materials have gained considerable interest because of their good charge transport characteristics, high optical characteristics and tunable electronic characteristics, which altogether make them have high device efficiencies and versatility [6, 7].

Modern developments in halide perovskites (HPs), specifically lead-based hybrid forms such as $CH_3NH_3PbX_3$ (X = I, Br), have received significant interest due to their exceptional optical properties and improved photovoltaic characteristics [8, 9]. In 2012, Kim et al. [10] stated a substantial development in the efficiency of $CH_3NH_3PbI_3$ power conversion (PCE) with values greater than 9 percent. Due to the continuous development of material design and device engineering, today the PCE has surpassed 25% [11, 12], and these perovskite solar cells have become similar to other established silicon and cadmium telluride-based photovoltaic technologies [12-14]. Guo et al. have recently employed an extremely efficient vapor-deposition method to construct stable lead-based perovskite solar cells ($CsPbBr_3$) successfully upon the discovery of an appropriate molecular ionic liquid by means of computer simulations. [15]. To solve the health and environmental challenges brought about by lead poisoning, B-site Pb is often substituted with more environmental friendly cations, including Ge, Bi, Ag, In, or Sb in perovskite-based structures [16, 17]. The alternatives of Pb-based perovskites are supposed to possess desirable optoelectronic properties, structural stability in the long run, mechanical flexibility, and scalability [18]. These compounds have a chemical formula of $A_2BB'X_6$, and the quaternary halide perovskites are obtained by replacing the combination of monovalent (B), and trivalent (B′) cation by the toxic $Pb^{2+}$ ions. This compensatory substitution is a charge-compensating substitution that is highly effective in decreasing the toxicity and preserving the structural integrity. The A-site cations in these compounds are usually a member of the alkali metal group, the X anions are of the halogen group and the B and $B^+$ cations are based on transition metals or pnictogens. $Cs^+$ ions are most commonly observed in the A-site because of their ability to enhance the structural stability, as well as prevent the structure breakdown. It is also remarkable that, when $Cs^+$ ions are included, the overall lattice stability is enhanced by strengthening the bond between the A-site and the octahedral [$BX_6$] framework [19, 20]. Equally, the Pb atom at the B-site is often substituted with less toxic cations such as Ge, Bi, Ag, In, or Sb, to ease the issue of toxicity [21]. Halide perovskites based on cesium have received much interest because of their exceptional structural and optoelectronic merits. Specifically, the compounds of the overall structure $Cs_2B^+B'^{3+}X_6$, have been widely studied both theoretically and experimentally on their promise in a variety of industrial applications [22]. $Cs_2AgBiBr_6$ was found to have an indirect band gap of 1.95 eV, so that it can be used as a potential material to act as a top absorber layer in a tandem solar cell system. [23]. Diverse tunable optical, structural and electrical properties are found in double perovskite compounds with thallium. According to Murtaza et al. (2024), $Cs_2AlTlH_6$ has an indirect band gap of 2.38 eV, which rises to 2.51 eV when spin-orbit coupling is included. In contrast, $Cs_2NaInH_6$ shows indirect gaps of 3.34 eV and 3.40 eV [24]. $Cs_2LiTlBr_6$ and $Cs_2NaTlBr_6$ have direct band gaps at the Γ point of approximately 1.82 eV, which means they have a very high solar potential [25]. Also, Hasan et al. have found out that $Cs_2NaTlX_6$ (X = F, Cl, Br) is a direct band gap material with significant dielectric properties which are established by its absorption, reflectivity and index of refraction [26]. Furthermore, $Cs_2AgInCl_6$, which has a direct band gap of 3.57 ± 0.03 eV and is more stable than $Cs_2AgSbCl_6$, which degrades rapidly but has an indirect band gap of 2.57 ± 0.05 eV, was demonstrated by Dahl et al. (2019) using experiments and density functional theory [27].

According to all these DFT-based studies, thallium-based double perovskites have potential in the thermoelectric, photovoltaic, photocatalytic, and UV optoelectronic. Thallium-based double perovskites have been the focus of significant interest because of their tunable structural, electronic

and optical characteristics, and present an opportunity to be used in photovoltaic and optoelectronic applications. It has been shown by a number of theoretical studies that Tl-based double perovskites have appropriate band gaps, desirable dielectric behavior and desirable charge transport properties. Specifically, $Cs_2LiTlBr_6$, $Cs_2NaTlBr_6$, and Cs2NaTlX6 (X = F, Cl, Br) have demonstrated good optoelectronic characteristics. Moreover, the addition of $Al^{3+}$ cations can increase the structural stability because they have an appropriate ionic radius and high bonding properties. The double perovskite $Cs_2AlTlX_6$ (X = F, I) will be motivated by these benefits as it is projected to have desirable structural stability and optoelectronic properties.

However, to the best of our knowledge, this compound has not yet been investigated using either experimental or theoretical approaches. Thus, a first-principles study of $Cs_2AlTlX_6$ (X=F, I) is conducted thoroughly in this work to investigate its structural, electronic, elastic and optical characteristics, and also assess its suitability in optoelectronic and energy related applications. In this article, the detailed study of the theoretical investigation of the double perovskite $Cs_2AlTlX_6$ (X=F, I) is done based on the density functional theory. As far as we know, this compound has not been studied either by computational or experimental techniques. Its optical response, electrical properties, and structural stability will be analyzed to help provide an insight into its potential application in energy conversion and optoelectronic devices.

**Computational Methodology**

This paper used Density Functional Theory (DFT) to evaluate the structural, electronic, optical and the elastic characteristics of the material. DFT is an effective and popular computing technique used to study new materials because of its high success in predicting physical properties of materials [28]. It enables evaluation of the various phenomena including structural, elastic, electronic, optical and thermoelectric properties [29-31]. The structural optimization and electronic structure calculations were done using the assistance of WIEN2k, which is a computer software that is based on the full-potential linearized augmented plane wave (FP-LAPW) technique [32]. Computation of the Kohn-Sham equations was done based on the self-consistency of full-potential linearized augmented plane wave (FP-LAPW) approach [33]. The exchange-correlation energy in Kohn-Sham formulation of the density functional theory (DFT) is a functional of the spin resolved densities of the electron density and needs to be computed. [34].The generalized gradient approximation or GGA provides a reliable accuracy to systems in which the electron densities change gradually. This paper has used Perdew-Burke-Ernzerhof (PBE-GGA) functional model to explain the exchange-correlation potential [34]. However, GGA is based on the basic properties of the material, and it is well known that GGA usually provides underestimates or even no prediction of the band gaps of insulators and semiconductors [34]. To overcome this shortcoming, the modified Becke-Johnson (mBJ) exchange potential was used in order to enhance the accuracy of the band-gap [33]. The mBJ functional produces a complete Hamiltonian with much more consistent band-gap values in comparison with the experimental ones by combining both the GGA exchange and correlation variables [33]. The mBJ potential was applied to obtain GGA correlation with it to make the band-gap estimation more accurate. The self-consistent computations were done using the energy convergence criterion of 0.01 Ry and 1000 k-point grid to ensure a high quality of the numerical precision and stability of the system [35].The plane-wave expansion cutoff was determined with the value $RMT \cdot Kmax = 7.0$, where RMT is the radius of the atomic sphere and Kmax is the plane-wave cutoff. Thermoelectric transport properties, namely the Seebeck coefficient (S), electrical conductivity ($\sigma/\tau$), electronic thermal conductivity ($\kappa_e/\tau$), and power factor ($PF/\tau=S^2(\sigma/\tau)$) were computed using the **BoltzTraP** code within the constant relaxation time approximation employing the TB-mBJ band structure, while the corresponding ZT values were estimated as a function of temperature under intrinsic-carrier conditions.

## Results and Discussion

### Structural Properties

The $Cs_2AlTlX_6$ (X = F, I) compounds exhibit a cubic double perovskite structure belonging to the Fm-3m space group (No. 225). The halogen atoms (X = F, I) are located at fractional coordinates (0.200963, 0, 0) and (0.226394, 0, 0), respectively, while the Al and Tl atoms occupy the (0, 0, 0) and (1/2, 0, 0) positions, respectively, and the Cs atoms are situated at the (1/4, 1/4, 3/4) positions. This symmetric arrangement forms a three-dimensional network of alternating [$AlX_6$] and [$TlX_6$] octahedra, with the lattice structure stabilized by Cs atoms. The crystal structure of $Cs_2AlTlX_6$ (X = F, I) was visualized using VESTA software [35], as shown in Figure 1(a, b).

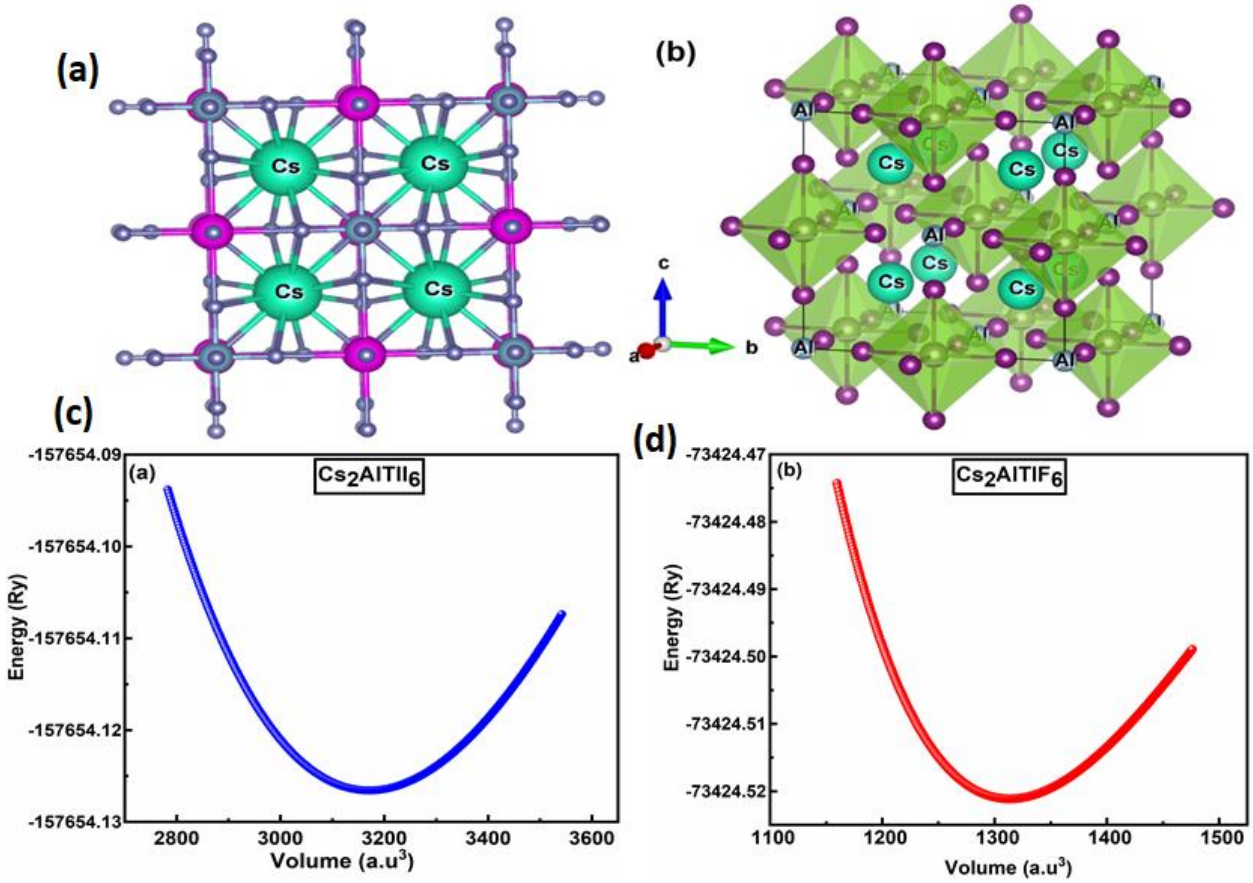


**Fig. 1:** Schematic representation of cubic perovskite structure of (a) $Cs_2AlTlI_6$ and (b) $Cs_2AlTlF_6$ Variation of total energy as a function of unit-cell volume for (c) $Cs_2AlTlI_6$ and (d) $Cs_2AlTlF_6$

The Birch-Murnaghan equation of state was employed to optimize the crystal structure of $Cs_2AlTlX_6$ (X = F, I) in order to determine the equilibrium lattice parameters and associated mechanical properties [36]. The well-defined minima in the energy–volume curves confirm the structural stability of both compounds in their optimized configurations as illustrated in Figure 1(c, d).

Compared to $Cs_2AlTlF_6$ ($a_0$ = 9.1995 Å, $V_O$ = 1313.5053 a.u³), $Cs_2AlTlI_6$ exhibits a larger equilibrium lattice constant ($a_0$ = 12.3048 Å) and unit cell volume ($V_O$ = 3170.8197 a.u³), as listed in

Table 1.
**Table 1:** Optimized structural parameters for $Cs_2AlTlX_6$ (X = F, I) double perovskite compounds.

| Parameters | $Cs_2AlTlI_6$ | $Cs_2AlTlF_6$ |
|---|---|---|
| **$a_0$ (Å)** | 12.3048 | 9.1995 |
| **$E_0$ (Ry)** | -157654.126576 | -73424.521141 |
| **$V_0$ (a.u.³)** | 3170.8197 | 1313.5053 |
| **B (GPa)** | 15.9505 | 50.0173 |
| **B′** | 4.5550 | 9.6789 |

This substituent effect of heavier halides on lattice constant is as expected due to the lattice expansion by the higher ionic radius of iodine. Conversely, the bulk modulus of $Cs_2AlTlF_6$ reduces to 15.9505 GPa ($Cs_2AlTlI_6$) and this shows that the fluorinated compound is not compressible and mechanically stiffer. The calculated pressure derivatives B′ are also supported by this behavior, B′ of $Cs_2AlTlF_6$ being 9.6789, and $Cs_2AlTlI_6$ being 4.5550. These findings in general indicate the structural stability of both optimized compounds, where $Cs_2AlTlF_6$ has a higher mechanical rigidity and $Cs_2AlTlI_6$ has a higher volumetric expansion because of the presence of the larger halide ion.

**Elastic Properties**

The elastic characteristics of the material are critical to their application in technical and engineering processes where structural stability, life cycle and mechanical strength are paramount. These properties influence the behavior of a material when it is subjected to various loading conditions by dictating the response of the material to the external loads and deformations [37]. The elastic constants of $Cs_2AlTlX_6$ (X= I, F) were calculated using the IRelast package [38] that is part of the WIEN2k code. The mesh was a 1000 k-point mesh, which gave high accuracy in self-consistent calculations. The obtained elastic constants ($C_{11}$, $C_{12}$, and $C_{44}$) confirm that both compounds satisfy the Born–Huang mechanical stability criteria for cubic systems, which require that $C_{11} - C_{12} > 0$, $C_{11} > 0$, $C_{44} > 0$, and $C_{11} + 2C_{12} > 0$. A comparative analysis reveals that $Cs_2AlTlF_6$ possesses significantly higher elastic stiffness, with $C_{11}$ = 91.27 GPa and $C_{44}$ = 25.82 GPa, compared to $Cs_2AlTlI_6$ ($C_{11}$ = 28.40 GPa, $C_{44}$ = 11.58 GPa). This implies that the fluorinated compound is more deformation-resistant and has superior stiffness.

**Table 2:** Elastic properties of $Cs_2AlTlX_6$ (X = I, F) compounds utilising the integrated IRelast module of the WIEN2k code.

| Elastic Parameters | $Cs_2AlTlI_6$ | $Cs_2AlTlF_6$ |
|---|---|---|
| **$C_{11}$** | 28.401930 | 91.265884 |
| **$C_{12}$** | 10.285196 | 27.918027 |
| **$C_{44}$** | 11.581933 | 25.816867 |
| **Y** | 26.088 | 70.926 |
| **G** | 10.49660057 | 28.0193416 |
| **A** | 1.279 | 0.815 |
| **v** | 0.234 | 0.259 |
| **B** | 16.333 | 49.122 |
| **B/G** | 1.556027582 | 1.753146119 |
| **$G_v$** | 10.573 | 28.160 |

The higher values of bulk modulus of 49.12 GPa of $Cs_2AlTlF_6$ and 16.33 GPa of $Cs_2AlTlI_6$ also indicate the stronger interatomic bond in the fluoride compound and the same trend is observed in the values of Young modulus (Y) and shear modulus (G), which indicates that this compound has better mechanical stiffness. The calculated ratios of Poisson's of $Cs_2AlTlI_6$ and $Cs_2AlTlF_6$ are 0.234 and 0.259, respectively; the smaller value of $Cs_2AlTlI_6$ is expected due to stronger directional bonding and higher brittle behavior and vice versa. Both compounds have elastic anisotropy, indicated by values of anisotropy factors of 1.279 $Cs_2AlTlI_6$ and 0.815 $Cs_2AlTlF_6$, respectively, with the iodide exhibiting slightly greater directional dependence. Mechanical behavior was additionally explained by the Cauchy pressure ($C_{12} - C_{44}$) and ratio of Pugh (B/G). $Cs_2AlTlI_6$ displays negative Cauchy pressure and a B/G ratio that is less than the critical value of 1.75, which proves its brittle nature. Conversely, $Cs_2AlTlF_6$ exhibits positive Cauchy pressure with slightly better B/G ratio, which reflects a ductile behavior that is on the brittle to ductile borderline with a slight enhanced ductility. On the whole, the replacement of fluorine increases stiffness, elastic resilience, and mechanical strength, and $Cs_2AlTlF_6$ can be used in the area that needs larger structural integrity.

The higher interatomic bonding strength is further highlighted by bulk modulus (B) of 49.12 GPa of $Cs_2AlTlF_6$ and 16.33 GPa of $Cs_2AlTlI_6$; the same is reiterated by the value of the Young's modulus (Y) and shear modulus (G). The Poisson ratios of the iodide and fluoride of 0.234 and 0.259, respectively, are within the normal range of 0.25- 0.50, which evidences that strong central bonding forces exist in both compounds. The anisotropy factor (A) values of 1.279 $Cs_2AlTlI_6$ and 0.815 $Cs_2AlTlF_6$ confirm the presence of anisotropic behavior in both cases (although the anisotropy of the elastic behavior is slightly higher in the iodide). A negative value of $C_{12}$, $C_{44}$ implies that the material is brittle, whereas a positive value of $C_{12}$ $C_{44}$ implies ductile behavior. But $Cs_2AlTlF_6$ has a slightly positive ($C_{12} - C_{44}$) value, which indicates a moderately ductile behavior and mechanical stability, whereas $Cs_2AlTlI_6$ has a negative ($C_{12} - C_{44}$) value, and therefore is brittle. Another parameter that is used to distinguish between brittle and ductile materials is the B/G ratio; where 1.75 is a critical point. B/G ratios less than 1.75 are defined as brittle; whereas more than 1.75 as ductile. The negative ($C_{12} - C_{44}$) value of Cs 2AlTlI 6 in the present work signifies the brittle nature, whereas the ($C_{12} - C_{44}$) value of $Cs_2AlTlF_6$ is positive, which means it is slightly ductile and, therefore, stable in its mechanical behavior. This is within the Poisson ratio requirements of both brittle and ductile materials as explained by Frantsevich et al [38]. The net stiffness, ductile and elastic resilience increase due to the fluorine substitution implies that $Cs_2AlTlF_6$ is more mechanically robust than its iodide analog, and therefore more suitable in areas where flexible and mechanically stable electronic devices are required.

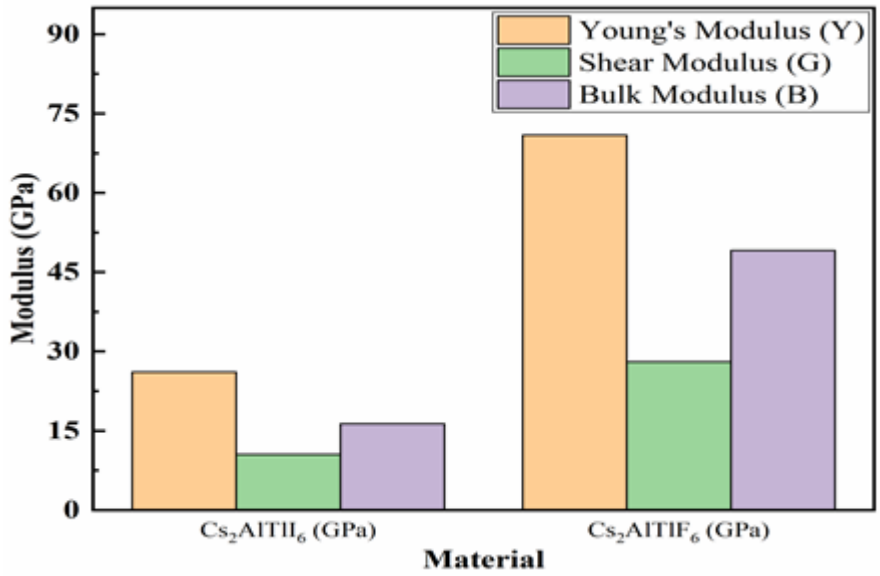


**Figure 2:** The Young's modulus (Y), bulk modulus (B), and shear modulus (G) of $Cs_2AlTlI_6$ and $Cs_2AlTlF_6$ are depicted in the comparison bar chart.

Figure 2 compares the Young's modulus (Y), shear modulus (G) and bulk modulus (B) of $Cs_2AlTlI_6$ and $Cs_2AlTlF_6$. $Cs_2AlTlF_6$ obviously shows greater elastic moduli than Cs 2 Al TlI 6, which is in line with greater interatomic bonding and mechanical stiffness. This increase in substitution by fluorine can be explained by the decreased atomic radius and increased electronegativity of F, which makes the Al–F and Tl–F bonds stronger compared to the weaker Al–I and Tl–I bonds in $Cs_2AlTlI_6$.

Figure 3 and Figure 4 depict the anisotropic elastic behavior of $Cs_2AlTlX_6$ (X= I, F) with 2D polar plot and 3D surface plot of Poisson ratio (nu), shear modulus (G) and Young modulus (E). These plots give a directional perspective of the elastic reaction above the scalar elastic constants. In both compounds, the elastic anisotropy is proven by departures of the perfect circular and the spherical symmetry. The deviation is also a little stronger in the case of $Cs_2AlTlI_6$ which has A = 1.279, and $Cs_2AlTlF_6$, A = 0.815, is somewhat closer to isotropic behavior even though there is still clear directional variation in the plotted surfaces.

Overall, the analysis of anisotropy shows that the substitution of fluorine with its equivalent rises the elastic stiffness and mechanical strength and maintains moderate directional dependence in the elastic response. By contrast, the iodide analogue is softer and slightly more anisotropic. These trends which are direction dependent are significant in forecasting structural reliability under the external stress and are also relevant in the further support of the higher mechanical resilience of $Cs_2AlTlF_6$.

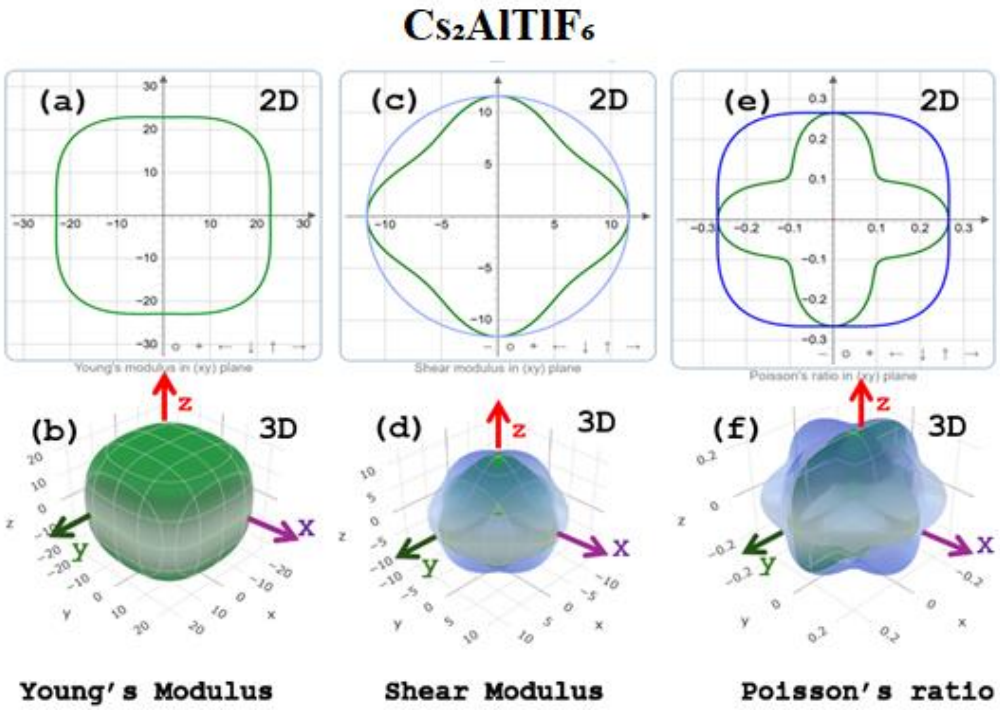


**Figure 3 :**( a–f) Young's modulus, shear modulus, and Poisson's ratio are plotted in 2D polar and 3D surface plots to demonstrate the anisotropic elastic properties of $Cs_2AlTlF_6$.

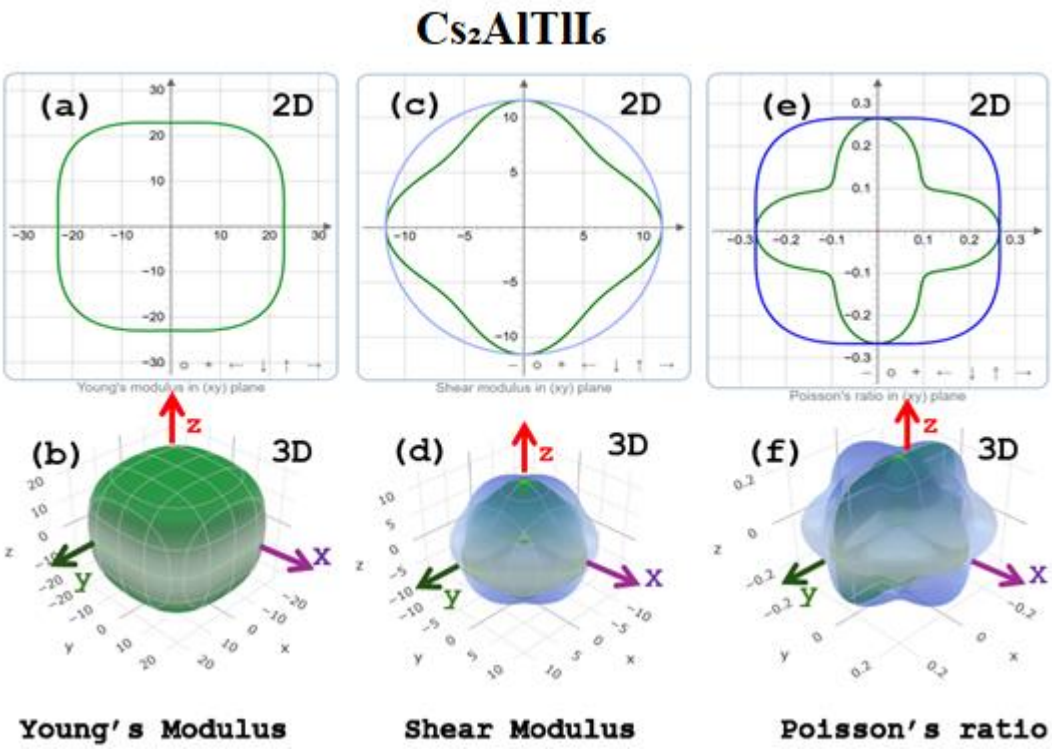


**Figure 4:** (a–f) Young's modulus, shear modulus, and Poisson's ratio are plotted in 2D polar and 3D surface plots to demonstrate the anisotropic elastic properties of $Cs_2AlTlI_6$.

These results show that both halide double perovskites are mechanically stable; conversely, $Cs_2AlTlF_6$ is more rigid, elastic, and structurally robust than its iodide counterpart, making it a better choice for applications requiring great mechanical durability.

**Electronic Properties**

The electronic properties of $Cs_2AlTlX_6$ (X = F, I) were determined by computing the electronic band structure and density of states of the material as presented in Figure 5. The findings indicate that the two compounds also have indirect band gaps with the valence-band maximum (VBM) and conduction-band minimum (CBM) located at non-overlapping high-symmetry positions in the Brillouin zone. The band gap of $Cs_2AlTlF_6$ is calculated to be 7.8 e V, which means that it is an insulator with a very broad band gap. This large energy gap does not allow excitation of electrons at normal temperatures, which proves that it is a strong insulator. Conversely, $Cs_2AlTlI_6$ with an indirect band gap of 2.97 eV is in the semiconducting range and indicates that it could be used in optoelectronic and ultraviolet-visible photonic applications. It is the greater ionic radius and stronger orbital hybridization of iodine over fluorine that causes the reduction in band gap in $Cs_2AlTlF_6$ to $Cs_2AlTlI_6$ to increase orbital overlap and decrease the energy gap between the conduction and valence bands. Moreover, the fact that there are no electronic states at the Fermi level proves the non-metallic properties of the two compounds. According to these results, $Cs_2AlTlF_6$ can be discussed as a wide-band-gap insulator, and $Cs_2AlTlI_6$ can be discussed as a semiconductor with promising optoelectronic characteristics.

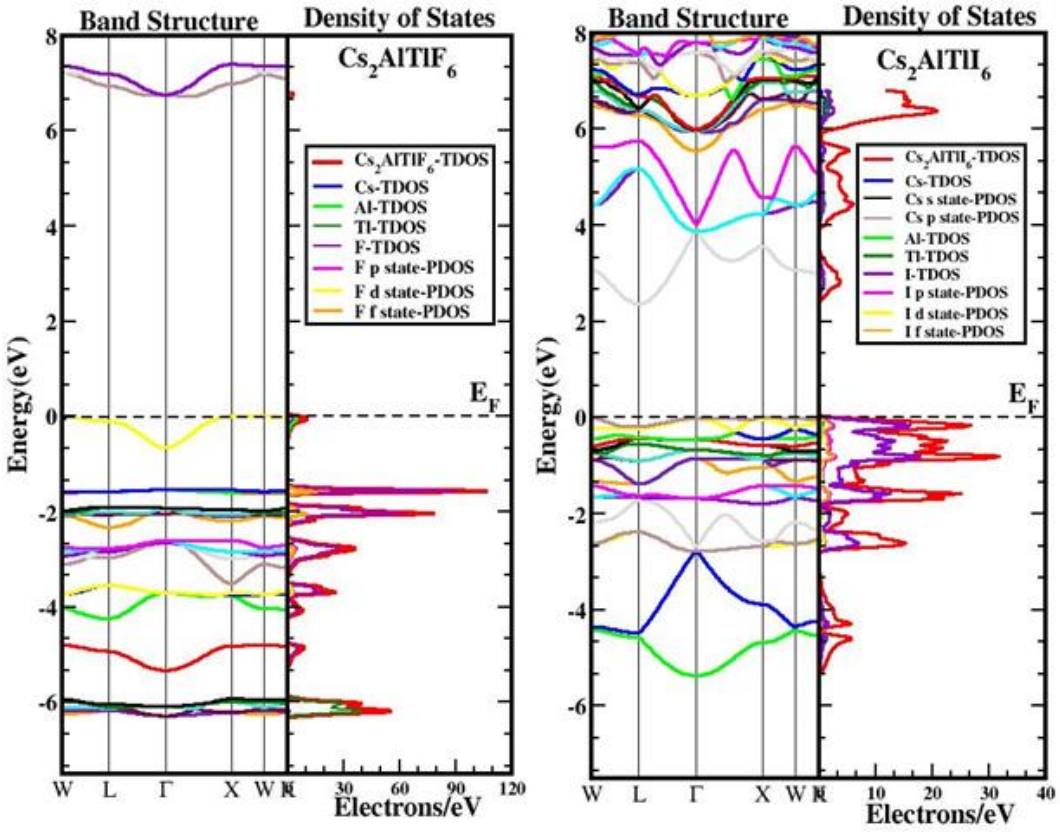


**Figure 5:** The total/partial density of states (TDOS and PDOS) and electronic band structures of $Cs_2AlTlX_6$ (X = I, F)

**Optical Properties**

Based on the theoretically optimized lattice constants, all optical properties were investigated, with special attention focused to the dielectric function ε (ω), which is defined as follows:

$$\varepsilon(\omega) = \varepsilon_1(\omega) + i\varepsilon_2(\omega) \qquad (1)$$

The refractive index, absorption coefficient, reflectivity, optical conductivity, and refraction were evaluated using the following mathematical expressions [39-41]:

$$n(\omega) = \frac{\sqrt{\{ [\, \varepsilon_1(\omega) + \sqrt{(\varepsilon_1{}^2(\omega) + \varepsilon_2{}^2(\omega))}\, ] \}}}{2} \qquad (2)$$

$$k(\omega) = \frac{\sqrt{\{ [\, -\varepsilon_1(\omega) + \sqrt{(\varepsilon_1{}^2(\omega) + \varepsilon_2{}^2(\omega))}\, ] \}}}{2} \qquad (3)$$

$$I(\omega) = \frac{2\omega k(\omega)}{c} \qquad (4)$$

$$R(\omega) = \frac{[\,(1 - n(\omega))^2 + k^2(\omega)\,]}{[\,(1 + n(\omega))^2 + k^2(\omega)\,]} \qquad (5)$$

$$\sigma(\omega) = \frac{(2W\, e\, \nu\, \hbar\, \omega)}{E_0} \qquad (6)$$

The TB-mBJ method was used to solve the dielectric function based on the optimized lattice constants in order to assess the basic optical properties of $Cs_2AlTlX_6$ (X = I, F) within the photon energy range of 0–40 eV.

**Dielectric Properties**

The optical characteristics of $Cs_2AlTlX_2$ (X = I, F) were measured using complex dielectric function in the photon energy spectrum 0-40 eV. Dielectric function ε (ω) has two parts, the real part $\varepsilon_1$ (ω) and the imaginary part $\varepsilon_2$ (ω). The actual component $\varepsilon_1$ (ω) is the response to an external electric field

of the material to dispersion and polarization, and the imaginary component $\varepsilon_2$ (ω) is related to interband electronic transitions and optical absorption. At low photon energies, $Cs_2AlTlI_6$ exhibits a comparatively larger static dielectric constant $\varepsilon_1$ (0) than $Cs_2AlTlF_6$, consistent with its larger static refractive index. The highest feature in $\varepsilon_1$ (ω) is at the 6 eV of $Cs_2AlTlF_6$, whereas $Cs_2AlTlI_6$ exhibits a sharp increase with a steady rise in energy. The interband electrons transitions between the valence and conduction bands are observed to be significantly higher between the ranges of 5 and 12 eV, and these are denoted by significant peaks in $\varepsilon_2$ (ω). Both $\varepsilon_1$ (ω) and $\varepsilon_2$ (ω) are lower than 15eV, which means that there is a lower likelihood of optical transitions occurring at higher energies. The strong dielectric response in the broad energy spectrum indicates that of $Cs_2AlTlX_2$ (X = I, F) double perovskite would be an excellent material to use in optoelectronics and high-frequency optics.

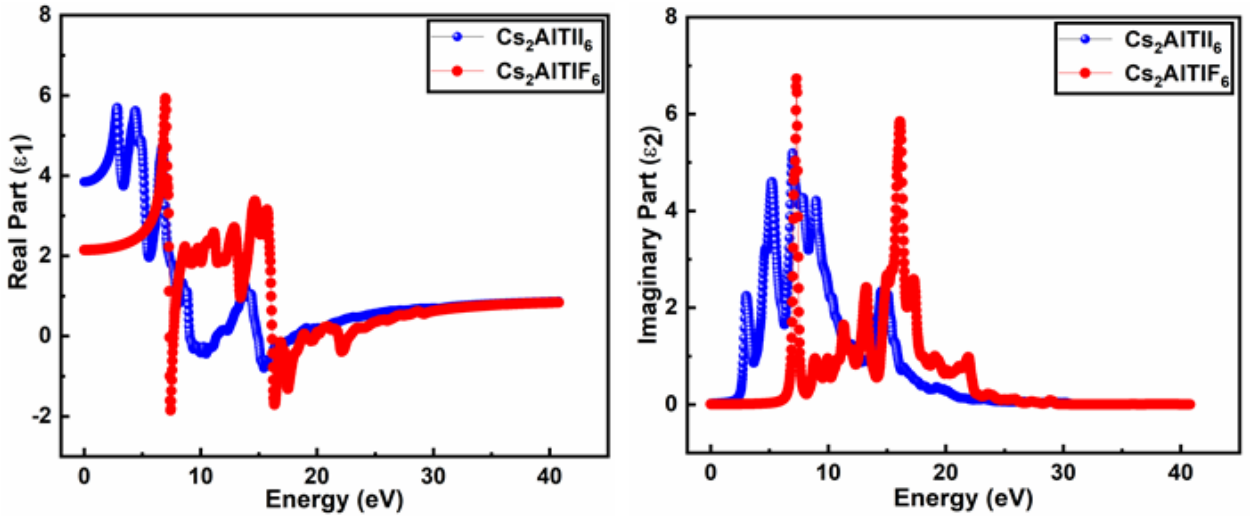


**Figure 6:** Dielectric function as a function of photon energy for $Cs_2AlTlX_6$ (X = I, F) compounds.

**Optical Conductivity**

Optical conductivity, σ (ω), offers valuable information about the electromagnetic radiation response of a material in its electronic behavior. It is directly connected to the interband electronic transitions taking place as a result of photons and the capacity of the material to absorb an incident. Figure 7(a) is the optical conductivity spectra of $Cs_2AlTlF_6$ and $Cs_2AlTlI_6$ obtained by analyzing the dielectric function ε (ω). $Cs_2AlTlI_6$ has the optical conductivity starting at approximately 3 eV, which is close to its calculated band gap and therefore, provides support that it is a semiconductor. $Cs_2AlTlF_6$ in contrast exhibits optical conductivity to emerge at a higher photon energy, which is in line with its insulating nature of wide-bandgap. $Cs_2AlTlF_6$ shows a sharp conductivity peak at 12 eV of around 13 000 $\Omega^{-1}$ $cm^{-1}$, with $Cs_2AlTlI_6$ having a similar peak of around 7000 $\Omega^{-1}$ $cm^{-1}$. These peaks are as a result of interband transitions among occupied valence-band states and vacant conduction-band states. Both compounds have a high level of light-matter interaction as shown by the finite optical conductivity over a wide energy range. Such outcomes indicate that $Cs_2AlTlI_6$ is a promising material to use in the optoelectronics industry, and $Cs_2AlTlF_6$ is more likely to be used in the ultraviolet photonic devices due to its large band gap.

**Absorption Coefficient**

Figure 7(b) displays the spectra of $Cs_2AlTlF_6$ and $Cs_2AlTlI_6$ absorption coefficient α (ω), of $Cs_2AlTlF_6$ and $Cs_2AlTlI_6$ obtained as the complex dielectric function ε (ω). The compounds both exhibit a high absorption in the photon-energy range of 0-40 eV. Consistent with the calculated electronic band gaps, the absorption edge of $Cs_2AlTlI_6$ occurs at the lower photon energy and $Cs_2AlTlF_6$ is moved to the higher photon energy ultraviolet region. $Cs_2AlTlI_6$ demonstrates a high level of absorption at 8 eV with the peak of 180 and $Cs_2AlTlF_6$ has the first major peak at 10 eV with

the peak of 297. The smaller peaks of 15-25 eV in the two materials also confirm the existence of more energetic interband transitions. The higher and wider ultraviolet absorption response of $Cs_2AlTlF_6$ suggests that more energy is interacting with the electron under photon and high energy optoelectronics devices are feasible by both compounds.

**Reflectivity**

In order to determine more about the optical nature of $Cs_2AlTlF_6$ and $Cs_2AlTlI_6$, the reflectivity spectra R (ω) are presented in Figure 7(c). $Cs_2AlTlF_6$ and $Cs_2AlTlI_6$ have a static reflectivity of about 0.035 and 0.105 respectively, which means that $Cs_2AlTlF_6$ and $Cs_2AlTlI_6$ do not reflect very well in the low-energy region. The two materials exhibit high reflectivity characteristics of approximately 8 eV and 16 eV with the highest values of 0.39 of $Cs_2AlTlF_6$ and 0.363 of $Cs_2AlTlI_6$. The reflectivity of the two compounds gradually decreases at photon energies above 20 eV, indicating a decreased role of reflected radiation at high-energy. The poor reflectivity in the visible and near-ultraviolet implies that these materials could be useful in transparent optical coating, optical window, and ultraviolet photonic devices.

**Refractive Index**

The refractive index n (ω) gives important information about interactions between electromagnetic radiation and $Cs_2AlTlX_6$ (X = F, I) compounds. Figure 7(d) shows that both compounds show changes in the refractive index with photon-energy range of 0-40 eV. At zero photon energy, $Cs_2AlTlI_6$ and $Cs_2AlTlF_6$ have a static refractive index of about 1.96 and 1.46 respectively, suggesting a moderate low-energy optical response. $Cs_2AlTlI_6$ thus has the higher static refractive index, but $Cs_2AlTlF_6$ has a somewhat higher maximum value of approximately 2.5 around 7 eV. $Cs_2AlTlI_6$ has a maximum refractive index of approximately 2.36 at approximately 4.5 eV. These findings point to the fact that these two compounds have a significant light-matter interaction, with $Cs_2AlTlF_6$ exhibiting a better response to the refractive index at shorter wavelengths.

**Extinction Coefficient**

Figure 7(e) displays the extinction coefficient K (ω), which is a representation of optical absorption losses. The two compounds have very low values of extinction in the low-energy region (below 5 eV), meaning that they have low optical loss and are highly transparent. The K (ω) increases steeply with photon energy with maxima of about 1.4 at 9 eV in $Cs_2AlTlI_6$ and 1.78 at 16 eV in $Cs_2AlTlF_6$ and then tailing off gradually with increasing photon energy. These findings affirm that the two materials are highly optically active in the UV region and still remain transparent in the low-energy region, thus qualifying as good candidates in the implementation of optoelectronic and photonic devices.

**Energy Loss Function**

The energy-loss function, L (ω), characterizes the energy loss of fast electrons passing through the material and gives information on collective charge-carrier oscillations, the plasmons. Figure 7(f) shows the calculated energy-loss spectrum of $Cs_2AlTlF_6$ and $Cs_2AlTlI_6$ at 0-40 eV. The compounds have both loss peaks at high energies of 18-22 eV, which are bulk plasmon excitation energies. $Cs_2AlTlI_6$ has a big peak of about 18.5 eV with maximum intensity of about 3 and $Cs_2AlTlF_6$ has a bigger peak of about 22 with maximum intensity of about 5.1. Increased intensity of $Cs_2AlTlF_6$ plasmon-peak means more collective oscillation of electrons and increased interaction with electromagnetic fields. At energies above 25 eV, the loss function becomes much lower indicating a lesser energy dissipation and electron scattering. These results suggest that $Cs_2AlTlX_6$ double perovskites have stable dielectric properties, and they are suitable in the use of high-frequency electromagnetic radiation and UV photo-electronic equipment.

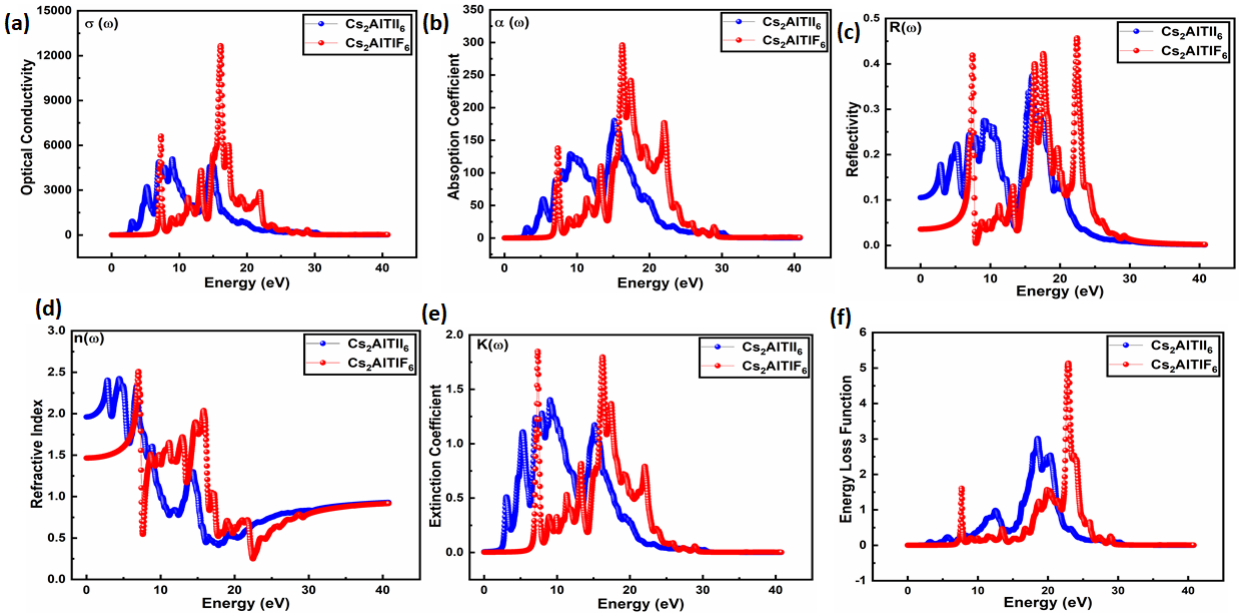


**Figure 7:** Optical conductivity (a), absorption coefficient (b), reflectivity R(ω) (c), refractive index n(ω) (d), extinction coefficient K(ω) (e), and energy-loss function L(ω) (f) of $Cs_2AlTlX_6$ (X = I, F).

**Thermoelectric Properties**

The thermoelectric behavior of $Cs_2AlTlI_6$ and $Cs_2AlTlF_6$ was estimated over the temperature range 100–1000 K, and the calculated transport coefficients are depicted in Figure 8(a–e). It is observed that the two compounds show a sharp contrast in all the transport quantities, which means that the substitution of halides has a strong impact on the thermoelectric response. Figure 8(a) is the electrical conductivity divided by relaxation time, σ /τ, which is significantly larger in $Cs_2AlTlF_6$ throughout the entire temperature range, but decreases slowly with temperature. By comparison, $Cs_2AlTlI_6$ is a low temperature, thermally activated semiconducting transport material with 6 showing very low σ/τ. The electronic thermal conductivity, $\kappa_e/\tau$, displayed in Figure 8(b), increases monotonically for both materials with increasing temperature, as expected from the correlation between charge transport and electronic heat conduction. However, the Seebeck coefficient S, shown in Figure 8(c), provides the most decisive distinction between the two compounds. $Cs_2AlTlI_6$ exhibits a remarkably large positive Seebeck coefficient throughout the entire temperature range, with a high value at low temperature that decreases gradually as temperature rises, indicating dominant p-type transport. By comparison, $Cs_2AlTlF_6$ shows an almost negligible Seebeck coefficient over the full range, which severely limits its thermoelectric usefulness despite its higher conductivity.

As can be seen in Figure 8(b), the electronic thermal conductivity, $\kappa_e/\tau$, rises steadily with temperature in both materials as would be expected based on the relationship between charge transport and electronic heat conduction. However, the Seebeck coefficient S, as Figure 8(c) gives, gives the clearest difference of the two compounds. $Cs_2AlTlI_6$ has an exceptionally large positive Seebeck coefficient over the entire temperature range, having a large value of the coefficient at low temperature which progressively decreases with increasing temperature, suggesting that transport is mainly p-type. Comparatively, $Cs_2AlTlF_6$ exhibits nearly zero Seebeck coefficient throughout the entire range, and this is highly detrimental to its thermoelectric utility even though it has a higher conductivity.

Since $PF/\tau = S^2 (\sigma/\tau)$, it is sensitive to the balance between thermopower and electrical conductivity. Figure 8(d) demonstrates that $Cs_2AlTlI_6$ has a power factor that increases strongly with temperature and is much larger than $Cs_2AlTlF_6$ at high temperatures. This improvement is a result of co-existence of a large Seebeck coefficient and steadily increasing conductivity. Conversely, the power factor of $Cs_2AlTlI_6$ is insignificant as the $S^2$ term is suppressed by it's near-zero Seebeck coefficient.

Figure 8(e) presents the estimated value of the dimensionless figure of merit, ZT, as a result of the sum of all of these transport coefficients. $Cs_2AlTlI_6$ exhibits a near temperature insensitive estimated ZT value near one over the temperature range studied, with a minor decrease at higher temperatures, a positive and predictable thermoelectric trend. $Cs_2AlTlF_6$ on the contrary has a very small estimated ZT over the entire range studied, and only a slight rise at high temperature. This is due to its poor performance which is mainly caused by its disappearing thermopower which highly suppresses the power factor although it has a relatively large conductivity.

Overall, the results shows, $Cs_2AlTlI_6$ as the best thermoelectric material. Replacement of F with I results in a desirable balance of high thermopower, power factor increasing and an estimated figure of merit that is constant, and the fluoride analogue does not provide useful thermoelectric efficiency due to its insignificant Seebeck response. These results indicate that halide engineering can be a useful tool to tune the transport properties of the double perovskites and $Cs_2AlTlI_6$ is a promising material to be used in medium- to high-temperature thermoelectric devices.

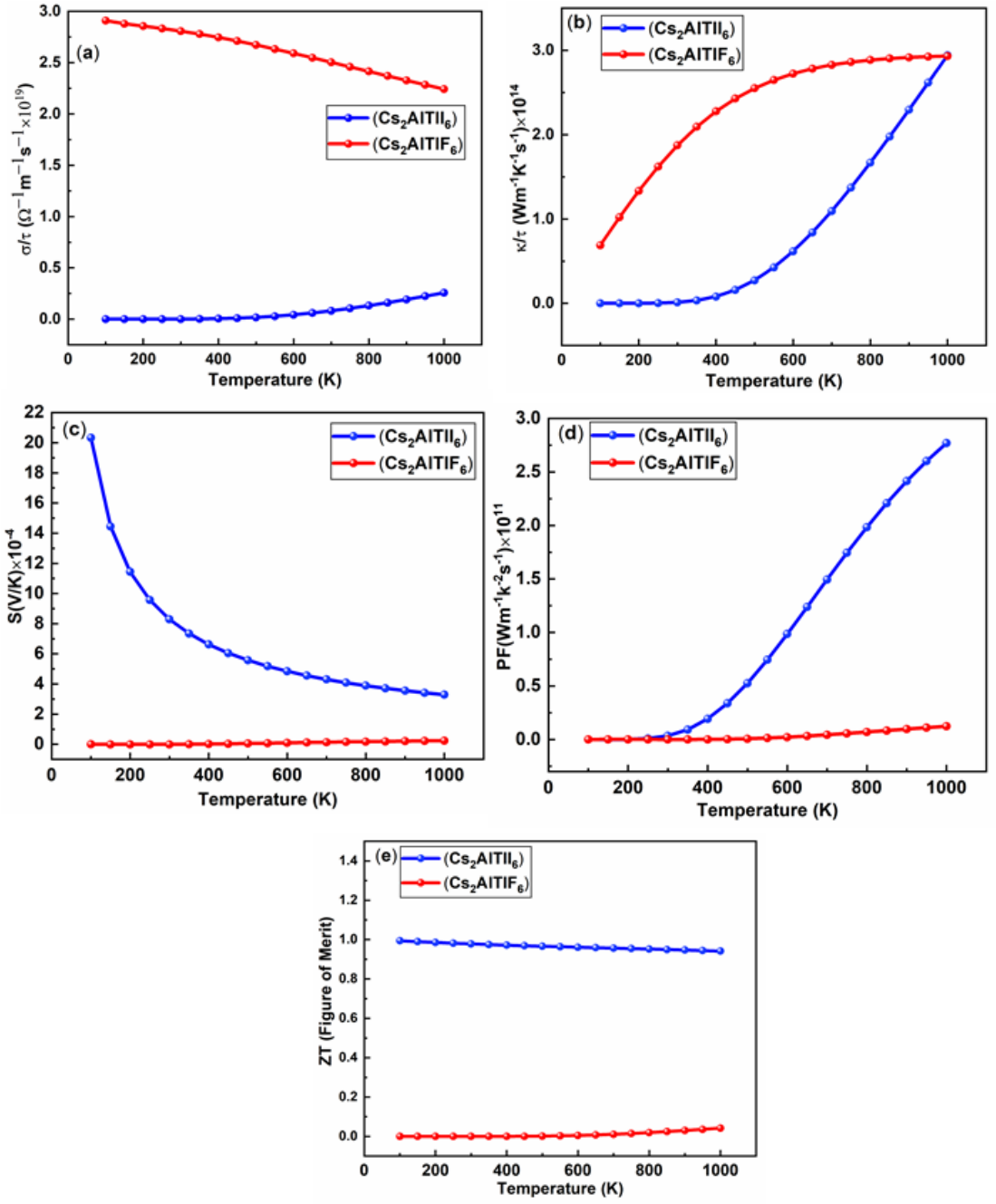


**Figure 8:** Thermoelectric properties of $Cs_2AlTlX_6$ (X = I, F) cubic double perovskites

## Conclusion

Overall, a detailed first-principles study of $Cs_2AlTlX_6$ (X=I, F) double perovskites was conducted to understand their structural, elastic, electronic, optical, and thermoelectric properties. Both the compounds stabilize in the cubic Fm-3m structure and give good structural stability following geometry optimization. The iodide compound has a larger equilibrium lattice constant and unit-cell volume, but much higher bulk modulus, which means that it is more rigid and compressible. Elastic-constant analysis substantiates the fact that the two systems meet the Born-Huang mechanical stability criteria. Electronic-structure calculations based on the TB-mBJ potential reveal indirect band gaps of 2.97 eV for $Cs_2AlTlI_6$ and 7.8 eV for $Cs_2AlTlF_6$, classifying $Cs_2AlTlI_6$ as a semiconducting material with potential for optoelectronic applications and $Cs_2AlTlF_6$ as a wide-band-gap insulating material suitable for ultraviolet photonic applications. The optical properties such as dielectric function, optical conductivity, absorption coefficient, reflectivity, refractive index, extinction coefficient, and energy-loss function have been calculated and indicate that there is a significant light-matter interaction in the wide range of photon-energy. Thermoelectric analysis indicates that $Cs_2AlTlI_6$ exhibits a large positive Seebeck coefficient, increasing power factor with temperature and the estimated figure of merit is nearly constant near unity over 100-1000 K, whilst $Cs_2AlTlF_6$ has weak thermoelectric performance due to its very small Seebeck coefficient that dominates the power factor despite its relatively high electrical conductivity. The results indicate that halide substitution is an efficient pathway to tune the multifunctional characteristics of $Cs_2AlTlX_6$ double perovskites and $Cs_2AlTlI_6$ is the more promising perovskite to use in thermoelectric and optoelectronic applications, with $Cs_2AlTlF_6$ being more compatible with the environment of mechanical robust ultraviolet optical devices.

## References


[1] J. Breternitz, et al., Mechanochemical synthesis of the lead-free double perovskite Cs2[AgIn]Br6 and its optical properties, J. Phys. Energy 1 (2019) 025003.

[2] A. Kojima, et al., Organometal halide perovskites as visible-light sensitizers for photovoltaic cells, J. Am. Chem. Soc. 131 (2009) 6050-6051.

[3] E.T. McClure, et al., Cs2AgBiX6 (X = Br, Cl): New visible-light-absorbing, lead-free halide perovskite semiconductors, Chem. Mater. 28 (2016) 1348-1354.

[4] R.S. Lamba, et al., Band gap engineering in Cs2(NaxAg1-x)BiCl6 double perovskite nanocrystals, J. Phys. Chem. Lett. 10 (2019) 5173-5181.

[5] S. Adjokatse, H.-H. Fang, M.A. Loi, Broadly tunable metal halide perovskites for solid-state light-emission applications, Mater. Today 20 (2017) 413-424.

[6] J. Chen, et al., Crystal organometal halide perovskites with promising optoelectronic applications, J. Mater. Chem. C 4 (2016) 11-27.

[7] A.L. Bibi, I. Nah, Y. Nah, et al., Lead-free halide double perovskites: Toward stable and sustainable optoelectronic devices, Mater. Today 49 (2021) 123-144.

[8] M.Y. Sofi, M.S. Khan, J. Ali, M. Ajmal Khan, Exploring the lead-free halide Cs2MGaBr6 (M = Li, Na) double perovskites for sustainable energy applications, Sci. Rep. 14 (2024) 5520.

[9] Y. Shao, Y. Yuan, J. Huang, Correlation of energy disorder and open-circuit voltage in hybrid perovskite solar cells, Nat. Energy 1 (2016) 15001.

[10] H.-S. Kim, et al., Lead iodide perovskite sensitized all-solid-state submicron thin-film mesoscopic solar cell with efficiency exceeding 9%, Sci. Rep. 2 (2012) 591.

[11] H. Wei, et al., Lead-free hybrid perovskite N(CH3)4SnI3 with robust ferroelectricity induced by large and non-polar N(CH3)4+ molecular cation, Nat. Commun. 12 (2021) 637.

[12] Y. She, et al., Identifying and passivating killer defects in Pb-free double Cs2AgBiBr6 perovskite, J. Phys. Chem. Lett. 12 (2021) 10581-10588.

[13] W.S. Yang, B.-W. Park, E.H. Jung, N.J. Jeon, Y.C. Kim, D.U. Lee, S.S. Shin, J. Seo, E.K. Kim, J.H. Noh, Iodide management in formamidinium-lead-halide-based perovskite layers for efficient solar cells, Science 356 (2017) 1376-1379.

[14] W. Ke, C.C. Stoumpos, I. Spanopoulos, M. Chen, M.R. Wasielewski, M.G. Kanatzidis, Diammonium cations in the FASnI3 perovskite structure lead to lower dark currents and more efficient solar cells, ACS Energy Lett. 3 (2018) 1470-1476.

[15] R. Guo, J. Xu, H. Gu, X. Chu, Y. Zhao, X. Meng, Z. Wu, J. Li, Y. Duan, Z. Li, Z. Wen, S. Chen, Y. Cai, C. Liang, Y. Shen, G. Xing, W. Zhang, G. Shao, Effective defect passivation with a designer ionic molecule for high-efficiency vapour-deposited inorganic phase-pure CsPbBr3 perovskite solar cells, J. Mater. Chem. A 11 (2023) 408-418.

[16] F. Elfatouaki, O. F., E. Ibnouelghazi, D. Abouelaoualim, A. Outzourhit, Electronic and optical properties of CsGeX2M (X, M = Br, Cl, I) perovskites for solar cell applications: First-principles study using PBE and TB-mBJ potentials, Mater. Sci. Semicond. Process. 143 (2022) 106488.

[17] Y. Bekenstein, J.C. Dahl, J. Huang, W.T. Osowiecki, J.K. Swabeck, E.M. Chan, P. Yang, A.P. Alivisatos, The making and breaking of lead-free double perovskite nanocrystals of cesium silver-bismuth halide compositions, Nano Lett. 18 (2018) 3502-3508.

[18] Z. Zhang, J. Song, J. Hou, Z. Lin, Z. Hu, J. Chang, J. Zhang, Y. Hao, Potential applications of halide double perovskite Cs2AgInX6 (X = Cl, Br) in flexible optoelectronics: Unusual effects of uniaxial strains, J. Phys. Chem. Lett. 10 (2019) 1120-1125.

[19] B. Yang, J. Chen, F. Hong, X. Mao, K. Zheng, S. Yang, Y. Li, T. Pullerits, W. Deng, K. Han, Lead-free, air-stable all-inorganic cesium bismuth halide perovskite nanocrystals, Angew. Chem. Int. Ed. 56 (2017) 12471-12475.

[20] M.R. Filip, X. Liu, A. Miglio, G. Hautier, F. Giustino, Phase diagrams and stability of lead-free halide double perovskites Cs2BB'X6: B = Sb and Bi, B' = Cu, Ag, and Au, and X = Cl, Br, and I, J. Phys. Chem. C 122 (2018) 158-170.

[21] G. Volonakis, et al., Lead-free halide double perovskites via heterovalent substitution of noble metals, J. Phys. Chem. Lett. 7 (2016) 1254-1259.

[22] A.H. Slavney, et al., A bismuth-halide double perovskite with long carrier recombination lifetime for photovoltaic applications, J. Am. Chem. Soc. 138 (2016) 2138-2141.

[23] H. Murtaza, Q. ul Ain, J. Munir, H.M. Ghaithan, A.A.A. Ahmed, S.M. Qaid, Exploring the optoelectronic attributes, thermoelectric and photocatalytic potential of double perovskites Cs2BB'H6 (B = Al, Na and B' = Tl, In): A DFT study, Mater. Sci. Eng. B 301 (2024) 117171.

[24] M. Rehman, et al., First principles study of structural, electronic, elastic and optical properties of Cs2LiTlBr6 and Cs2NaTlBr6, Mater. Sci. Semicond. Process. 151 (2022) 106993.

[25] M.M. Hasan, N. Hasan, A. Kabir, First-principles studies on structural, electronic, optical and mechanical properties of inorganic Cs2NaTlX6 (X = F, Cl, Br) double halide perovskites, arXiv (2023) arXiv:2302.02201.

[26] J.C. Dahl, W.T. Osowiecki, Y. Cai, J.K. Swabeck, Y. Bekenstein, et al., Probing the stability and band gaps of Cs2AgInCl6 and Cs2AgSbCl6 lead-free double perovskite nanocrystals, Chem. Mater. 31 (2019) 3134-3143.

[27] I. de la Parra, et al., PV performance modelling: A review in the light of quality assurance for large PV plants, Renew. Sustain. Energy Rev. 78 (2017) 780-797.

[28] J.A. Camargo-Martínez, R. Baquero, Performance of the modified Becke-Johnson potential for semiconductors, Phys. Rev. B 86 (2012) 195106.

[29] M.S. Khan, et al., Investigation of structural, electronic and optical properties of potassium and lithium based ternary selenoindate using first-principles approach, J. Solid State Chem. 293 (2021) 121778.

[30] P. Blaha, K. Schwarz, G.K.H. Madsen, D. Kvasnicka, J. Luitz, WIEN2k: An Augmented Plane Wave Plus Local Orbitals Program for Calculating Crystal Properties, Vienna University of Technology, Vienna, Austria, 2001.

[31] P. Blaha, K. Schwarz, F. Tran, R. Laskowski, G.K.H. Madsen, L.D. Marks, WIEN2k: An APW+lo program for calculating the properties of solids, J. Chem. Phys. 152 (2020) 074101.

[32] F. Tran, P. Blaha, Accurate band gaps of semiconductors and insulators with a semilocal exchange-correlation potential, Phys. Rev. Lett. 102 (2009) 226401.
[33] J. Tao, H. Tang, J.P. Perdew, Origin of the size-dependence of the equilibrium van der Waals binding between nanostructures, J. Chem. Phys. 148 (2018) 074110.
[34] A. Ullah, et al., DFT study of structural, elastic and optoelectronic properties of binary X2Se (X = Cd, Zn) chalcogenides, Inorg. Chem. Commun. 174 (2025) 113985.
[35] K. Momma, F. Izumi, VESTA 3 for three-dimensional visualization of crystal, volumetric and morphology data, J. Appl. Crystallogr. 44 (2011) 1272-1276.
[36] F.D. Murnaghan, The compressibility of media under extreme pressures, Proc. Natl. Acad. Sci. U.S.A. 30 (1944) 244-247.
[37] S. Belhachi, et al., DFT analysis of Ba2NbRhO6: A promising double perovskite for sustainable energy applications, J. Inorg. Organomet. Polym. Mater. 35 (2025) 978-993.
[38] I.N. Frantsevich, F.F. Voronov, S.A. Bokuta, Elastic Constants and Elastic Moduli of Metals and Insulators, Naukova Dumka, Kiev, 1983.
[39] Q. Mahmood, et al., Study of new lead-free double perovskites halides Tl2TiX6 (X = Cl, Br, I) for solar cells and renewable energy devices, J. Solid State Chem. 308 (2022) 122887.
[40] D. Behera, S.K. Mukherjee, Optoelectronics and transport phenomena in Rb2InBiX6 (X = Cl, Br) compounds for renewable energy applications: A DFT insight, Chemistry 4 (2022) 1044-1059.
[41] N. Alaal, I.S. Roqan, Tuning the electronic properties of hexagonal two-dimensional GaN monolayers via doping for enhanced optoelectronic applications, ACS Appl. Nano Mater. 2 (2019) 202-213.